WATER RESOURCES RESEARCH, VOL. 49, 1–8, doi:10.1002/wrcr.20107, 2013

Vegetation control on water and energy balance within the Budyko framework

Dan Li,[1] Ming Pan,[1] Zhentao Cong,[2] Lu Zhang,[3] and Eric Wood[1]

Received 14 June 2012; revised 14 November 2012; accepted 13 January 2013.

[1] Budyko's framework has been widely used to study basin-scale water and energy balances and one of the formulations of the Budyko curve is Fu's equation. The curve shape parameter ϖ in Fu's equation controls how much of the available water will be evaporated given the available energy. Previous studies have found that land surface characteristics significantly affect variations in the parameter ϖ. In this study, we focus on the vegetation impact and examine the conditions under which vegetation plays a major role in controlling the variability of ϖ. Using data from 26 major global river basins that are larger than 300,000 km^2, the basin-specific ϖ parameter is found to be linearly correlated with the long-term averaged annual vegetation coverage. A simple parameterization for the ϖ parameter based solely on remotely sensed vegetation information is proposed, which improves predictions of annual actual evapotranspiration by reducing the root mean square error (RMSE) from 76 mm to 47 mm as compared to the default ϖ value used in the Budyko curve method. The controlling impact of vegetation on the basin-specific ϖ parameter is diminished in small catchments with areas less than 50,000 km^2, which suggests a scale-dependence of the role of vegetation in affecting water and energy balances. In small catchments, other key ecohydrological processes need to be taken into account in order to fully capture the variability of the ϖ parameter in Fu's equation.

Citation: Li, D., M. Pan, Z. Cong, L. Zhang, and E. Wood (2013), Vegetation control on water and energy balance within the Budyko framework, *Water Resour. Res.*, *49*, doi:10.1002/wrcr.20107.

1. Introduction

[2] Understanding the interactions between vegetation dynamics and the terrestrial water cycle under a changing climate is critical for many disciplines such as hydrology, meteorology, and ecology [*Eagleson*, 2002; *Rodríguez-Iturbe and Porporato*, 2004]. These complex interacting processes occur at various temporal and spatial scales. Over annual and longer temporal scales, Budyko's framework, which prescribes the dependence of actual evapotranspiration on energy availability (usually represented by the potential evaporation) and water availability (usually represented by the precipitation), is a useful tool to investigate the interplay between climate, vegetation, and the hydrologic cycle [*Donohue et al*., 2007, 2010; *Roderick and Farquhar*, 2011; *Wang and Hejazi*, 2011; *Yang and Yang*, 2011].

[3] Several analytical equations have been proposed for the Budyko curve [see *Yang et al*., 2008b for a review], among which the two one-parameter functions proposed by *Fu* [1981] [equation (1), see also *Zhang et al*., 2004] and *Choudhury* [1999] (equation (2)) are widely used:

$$\frac{E}{P} = 1 + \frac{E_p}{P} - \left[1 + \left(\frac{E_p}{P}\right)^{\varpi}\right]^{1/\varpi}, \tag{1}$$

$$\frac{E}{P} = \frac{E_p/P}{\left[1 + \left(E_p/P\right)^n\right]^{1/n}}, \tag{2}$$

where P, E_p, and E are the precipitation, potential evaporation, and actual evapotranspiration. E_p/P and E/P are also termed "dryness index" and "evaporation ratio," respectively. ϖ and n are empirical parameters that determine the shape of the Budyko curve and reflect the impact of other factors such as land surface characteristics and climate seasonality on water and energy balances. *Yang et al*. [2008b] theoretically derived Choudhury's equation (equation (2)) using Fu's method and showed that the two empirical parameters are related through $\varpi = n + 0.72$, implying the equivalence of the two analytical forms [see also *Sun*, 2007]. In this study, Fu's equation (equation (1)) is used.

[4] To use Fu's equation, the empirical parameter ϖ in equation (1) needs to be determined as a prior knowledge. For example, it can be calibrated from historical data. In ungauged basins where no calibration is possible, a simple parameterization for ϖ using available data sets is desirable. In Budyko's original hypothesis, the Budyko curve

[1]Department of Civil and Environmental Engineering, Princeton University, Princeton, New Jersey, USA.
[2]State Key Laboratory of Hydroscience and Engineering, Department of Hydraulic Engineering, Tsinghua University, Beijing, China.
[3]CSIRO Land and Water, Canberra, Australia.

Corresponding author: D. Li, Department of Civil and Environmental Engineering, Princeton University, Princeton, NJ 08540, USA. (danl@princeton.edu)

0043-1397/13/10.1002/wrcr.20107

was regarded as "universal" for all basins at long-term scale [*Budyko*, 1963, 1974], suggesting that only a single ϖ value is needed. The default Budyko curve method corresponds to a ϖ value of 2.6 [*Donohue et al*., 2011]. Later on, "basin-specific" Budyko curves were proposed: each basin has a distinct Budyko-type relationship between precipitation (P), potential evaporation (E_p), and actual evapotranpiration (E) at annual scale. That is, at annual scale, the shape parameter ϖ varies across different basins [*Sun*, 2007; *Yang et al*., 2007, 2009]. Consequently, a simple parameterization for ϖ with information that is readily available will be a good basis for applying Fu's equation and the Budyko framework.

[5] Several studies have demonstrated that ϖ is related to land surface characteristics, including vegetation, soil types, and topography, as well as climate seasonality [*Milly*, 1993, 1994; *Porporato et al*., 2004; *Shao et al*., 2012; *Williams et al*., 2012; *Yang et al*., 2007, 2009; *Yokoo et al*., 2008; *Zhang et al*., 2001, 2004]. In other words, given the same dryness index, land surface hydrology still varies due to variations in these factors. In particular, vegetation can serve as a good integrated indicator of these ecohydrological impacts on water and energy balances [*Donohue et al*., 2007] for many reasons. For example, the vegetation coverage reflects the effect of climate seasonality [*Gutman and Ignatov*, 1998]. Lower vegetation coverage might be associated with a large seasonal phase mismatch between precipitation and radiation, which is known to reduce the actual evapotranspiration [*Milly*, 1994; *Shao et al*., 2012; *Williams et al*., 2012; *Yokoo et al*., 2008]. Soil texture and topography regulate runoff generation and the water available for vegetation [*Shao et al*., 2012; *Williams et al*., 2012; *Yokoo et al*., 2008], thus embed their influences in vegetation signatures. Human activities such as harvesting, clearing, and fertilization alter both the vegetation and the evapotranspiration capacity [*Ma et al*., 2008; *Roderick and Farquhar*, 2011; *Wang and Hejazi*, 2011]. Some studies have investigated the role of vegetation in the Budyko framework. For example, leaf area index has shown a high correlation with the parameter ϖ in Fu's equation at the 10 day timescale [*Yang et al*., 2008a]. Including vegetation information improves the performance of the Budyko curve to a certain extent [*Donohue et al*., 2007, 2010]. *Shao et al*. [2012] used a multivariate adaptive regression spline model to estimate the model parameter and observed large impact of forest coverage on ϖ. *Yang et al*. [2009] parameterized ϖ using three nondimensional variables: the vegetation coverage derived from the normalized difference vegetation index (NDVI), the relative infiltration capacity (defined as the saturated hydraulic conductivity normalized by the mean precipitation intensity in a day, $K_s/\overline{i_r}$), and the average topographic slope ($\tan\beta$). However, the impact of vegetation coverage on the parameter ϖ is completely different in two groups of catchments: in the Hai River basin, the parameter ϖ is negatively correlated with the vegetation coverage while in the Yellow River basin and the Inland River basin, a positive correlation is observed. As a result, it is difficult to generalize the vegetation impact on the parameter ϖ and to apply their data-demanding parameterization for ϖ to other basins. Given that vegetation information reflects the integrated landscape and climatic features [*Donohue et al*., 2007] and the availability of global NDVI data sets, in this study, the relationship between the "basin-specific" Budyko curves and vegetation characteristics is investigated by using data sets that span a wide range of climate regimes and spatial scales; more specifically, under what conditions can the variability of ϖ be largely captured by vegetation information (i.e., NDVI) and whether a parameterization for ϖ based solely on NDVI can improve the performance of the Budyko approach are the foci of this work. The paper is organized as follows: section 2 describes the data and methodology; section 3 presents a simple parameterization for the basin-specific model parameter ϖ and its validation; section 4 presents the conclusions of the findings.

2. Data and Methodology

2.1. Data

[6] Basin averaged monthly time series of water budget terms, i.e., precipitation, evapotranspiration, runoff, and water storage changes, over 32 major river basins around the world from 1984 to 2006 are taken from the global water cycle assessment study of *Pan et al*. [2012]. The 32 river basins are: Amazon, Amur, Aral, Columbia, Congo, Danube, Dnieper, Don, Yellow, Indigirka, Indus, Kolyma, Lena, Limpopo, Mackenzie, Mekong, Mississippi, Murray-Darling, Northern Dvina, Niger, Nile, Ob, Olenek, Parana, Pechora, Senegal, Ural, Volga, Pearl, Yangtze, Yenisei, Yukon (see Figure 1 for the 26 river basins that are used in this study). *Pan et al*. [2012] collected and investigated estimates of the water budget terms from a wide range of sources, including in situ observations, remote sensing retrievals, land surface model (LSM) predictions, and reanalysis products. The study combined different data sources using data assimilation that weighted each source according to its estimated error and produced a unified estimate of the terrestrial water budget over these basins. The mass balance of water (i.e., water budget closure) was also enforced in the combined estimate through a constrained filtering technique [*Pan and Wood*, 2006]. The water budget estimates from *Pan et al*. [2012] is considered to be the best (highest confidence) estimates to date, given the data sources.

[7] Daily potential evaporation is calculated based on the Penman equation (cf., equation (3)) using the Princeton University global forcing data [*Sheffield et al*., 2006] that includes wind speed, relative humidity, air temperature, incoming short-wave and long-wave radiation, and LSM outputs (ground heat flux, outgoing short-wave and long-wave radiation) from the Variable Infiltration Capacity (VIC) LSM which is also driven by the Princeton University forcing [*Sheffield and Wood*, 2007]. The potential evaporation calculation follows [*Shuttleworth*, 1993]:

$$E_p = \frac{\Delta}{\Delta+\gamma}(R_n - G) + \frac{\gamma}{\Delta+\gamma}\frac{6430(1+0.54)(e_s - e_a)}{\lambda}, \quad (3)$$

where E_p is the potential evaporation (mm d^{-1}). Δ is the slope of the saturation vapor pressure curve (Pa K^{-1}), and γ is the psychometric constant (approximately 67 Pa K^{-1}); R_n is the net radiation and G is the ground heat flux (here in units of mm d^{-1}); e_s is the saturated water vapor pressure (Pa) while e_a is the actual water vapor pressure (Pa); u is the mean wind speed at 2 m above the ground (m s^{-1}); and

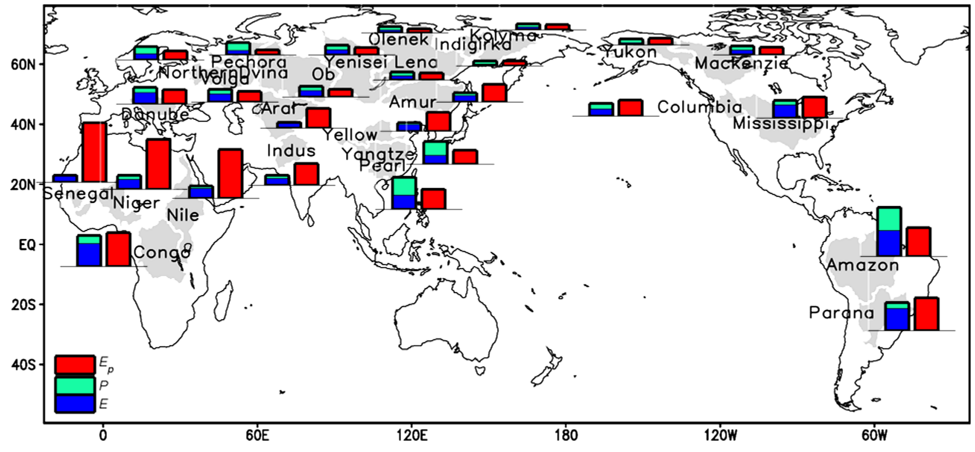

Figure 1. The map of 26 major basins over the globe and their long-term averaged annual precipitation, potential evaporation, actual evapotranspiration [*Pan et al*., 2012]. In Figure 1, actual evapotranspiration (blue) is shown as a portion of precipitation (green + blue). As a reference, the long-term averaged annual precipitation, potential evaporation, and actual evapotranspiration from Amazon basin are 2173, 1274, and 1145 mm, respectively.

λ is the latent heat of vaporization of water 2.45×10^6 (J kg^{-1}). The daily potential evaporation is aggregated to annual potential evaporation for the 32 basins.

[8] It is noted that more than 10% of data points from Dnieper, Don, Limpopo, Mekong, Murray-Darling, and Ural basins are outside the envelope that is constrained by the energy and water limits (see Figure 2). Hence these six basins are excluded in the following analyses. Basic characteristics of the remaining 26 basins are listed in Table 1. The areas of these 26 global river basins range from about 300,000 km^2 (Pechora) to about 6,000,000 km^2 (Amazon). The long-term averaged annual precipitation, potential evaporation, and actual evapotranspiration from the remaining 26 basins are also shown in Figure 1. It is clear that these 26 basins cover a large part of the world and span a wide range of climate regimes. The long-term averaged dryness index for the 26 basins ranges from 0.41 (Pechora) to 8.29 (Senegal) and the evaporation ratio ranges from 0.32 (Yukon) to 0.89 (Senegal). Figure 2 shows the long-term averaged evaporation ratios as a function of the long-term averaged dryness indices for the 26 global river basins. It can be seen that Fu's equation with a fitted ϖ value of 2.0 adequately captures the variations in the long-term water and energy balances in these basins.

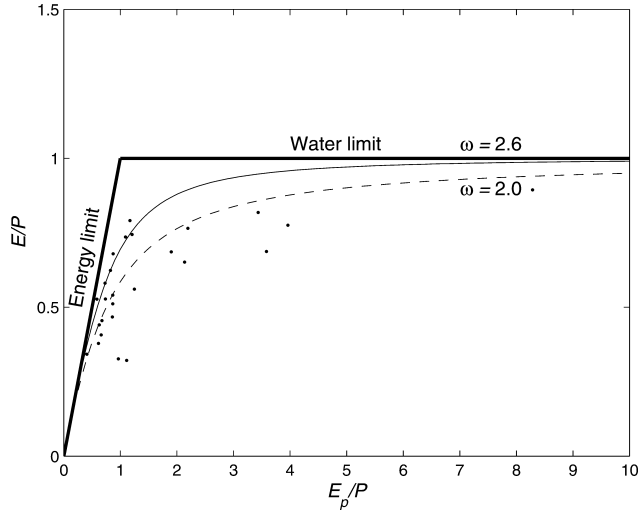

Figure 2. The long-term averaged annual evaporation ratios (E/P) in the 26 global river basins are plotted against the long-term averaged annual dryness indices (E_p/P). The bold black lines serve as an envelope (energy limit and water limit) to the Budyko curve family. The default Budyko curve corresponds to $\varpi = 2.6$ and $\varpi = 2.0$ is a fitted value using long-term averaged data.

Table 1. Basic Characteristics of the Selected 26 Global River Basins

Basin Number	Basin Name	Basin Area (10^6 km^2)	E_p/P	E/P	NDVI
1	Amazon	5.9	0.59	0.53	0.62
2	Amur	3.0	1.90	0.69	0.29
3	Aral	1.1	3.44	0.82	0.20
4	Columbia	0.7	1.25	0.56	0.34
5	Congo	3.7	1.09	0.74	0.60
6	Danube	0.8	0.87	0.68	0.47
7	Yellow	0.9	2.19	0.76	0.26
8	Indigirka	0.3	0.97	0.33	0.20
9	Indus	1.1	2.13	0.65	0.21
10	Kolyma	0.7	0.86	0.47	0.21
11	Lena	2.4	0.86	0.51	0.27
12	Mackenzie	1.7	0.87	0.54	0.32
13	Mississippi	3.2	1.21	0.74	0.43
14	Northern Dvina	0.4	0.68	0.45	0.45
15	Niger	2.2	3.59	0.69	0.25
16	Nile	3.8	3.96	0.78	0.28
17	Ob	2.6	0.73	0.58	0.35
18	Olenek	0.4	0.66	0.41	0.20
19	Parana	2.7	1.17	0.79	0.58
20	Pechora	0.3	0.41	0.34	0.29
21	Senegal	0.8	8.29	0.89	0.17
22	Volga	1.4	0.83	0.62	0.40
23	Pearl	0.4	0.63	0.44	0.43
24	Yangtze	1.8	0.61	0.38	0.39
25	Yenisei	2.6	0.74	0.53	0.32
26	Yukon	0.9	1.11	0.32	0.28

[9] The 10 km Global Inventory Modeling and Mapping Studies (GIMMS) NDVI data set, derived from the Advanced Very High Resolution Radiometer (AVHRR) sensor [*Buermann et al*., 2002], is used to represent the vegetation characteristics of the selected 26 global basins. Other vegetation information such as the vegetation optical depth [*Owe et al*., 2001] is also considered but does not provide clear advantages over NDVI. Long-term averaged (from 1984 to 2006) annual NDVI values are obtained from the data set, as shown in Table 1. The vegetation coverage (M) is calculated following *Yang et al*. [2009]:

$$M = \frac{\mathrm{NDVI} - \mathrm{NDVI}_{\min}}{\mathrm{NDVI}_{\max} - \mathrm{NDVI}_{\min}}, \tag{4}$$

where M indicates the vegetation coverage, $\mathrm{NDVI}_{\min}$ and $\mathrm{NDVI}_{\max}$ are chosen to be 0.05 and 0.8, respectively [*Yang et al*., 2009].

[10] Two additional data sets including 99 catchments in China [*Yang et al*., 2009] and 232 catchments in the United States are also used in this study. These catchments are significantly smaller than the 26 global river basins and the majority of these catchments have basin areas smaller than 50,000 km^2. The data set that includes 99 catchments in China spans from 1956 to 2000. *Yang et al*. [2009] reported the vegetation coverage and the parameter n values (note $\varpi = n + 0.72$). The 232 catchments in the United States were selected from a subset of watersheds included in the international Model Parameter Estimation Experiment (MOPEX) data set [*Duan et al*., 2006]. The MOPEX data set includes mean areal precipitation, potential evaporation, and daily streamflow data from 1948 to 2003 for 438 watersheds (ftp://hydrology.nws.noaa.gov) and has been used in many previous studies within the Budyko framework [*Wang and Hejazi*, 2011; *Wang and Alimohammadi*, 2012]. The 232 catchments are selected in this study so that each catchment has no missing data and have less than 10% data points outside the envelope that is constrained by the energy and water limits. This is identical to the selection criteria we employed for the global river basins. The MOPEX data set also includes greenness fraction which is similar to the vegetation coverage (M) and is also calculated using equation (4) based on NDVI information. The minor difference is that the $\mathrm{NDVI}_{\min}$ and $\mathrm{NDVI}_{\max}$ in the calculation are chosen to be 0.04 and 0.52 following the work by *Gutman and Ignatov* [1998]. In this study, the vegetation coverage for catchments in the MOPEX data set is recalculated using the greenness fraction and *Yang et al*.'s [2009] $\mathrm{NDVI}_{\min}$ and $\mathrm{NDVI}_{\max}$ values (i.e., 0.05 and 0.8, respectively).

2.2. Methodology

[11] If all the terms on both sides of Fu's equation (P, E, and E_p) are given for one basin for multiple years, then an optimal ϖ value for that basin can be inferred through a curve fitting procedure that minimizes the mean squared errors between the Budyko modeled annual evaporation ratios (E/P) and the measured ones. The objective function is:

$$\mathrm{Obj} = \min \sum_i \left\{ \frac{E_i}{P_i} - \left\{ 1 + \frac{(E_p)_i}{P_i} - \left[1 + \left(\frac{(E_p)_i}{P_i} \right)^{\varpi} \right]^{1/\varpi} \right\} \right\}^2, \tag{5}$$

where i is year. The parameter ϖ obtained in this way is called the "basin-specific ϖ" herein. These basin-specific ϖ values can then be used as the reference for creating a new ϖ parameterization based on vegetation information. The new ϖ parameterization is simply a linear regression between the fitted basin-specific ϖ and the long-term averaged annual vegetation coverage: $\varpi = a \times M + b$; where a and b are constants. The ϖ values estimated from vegetation coverage M using $\varpi = a \times M + b$ is called the "modeled ϖ" or ϖ_M herein.

[12] To assess the improvement of this new parameterization for ϖ in modeling annual evapotranspiration, we compare the annual evapotranspiration predictions from the Fu's equation using (1) the default ϖ value of 2.6, (2) the fitted ϖ value of 2.0, (3) the modeled ϖ from the long-term averaged annual vegetation coverage, and (4) the basin-specific ϖ, to the annual evapotranspiration estimates provided by *Pan et al*. [2012].

3. Results

3.1. Basin-Specific Budyko Curves

[13] Figure 3 presents the ratios of annual actual evapotranspiration to precipitation (E/P) as a function of annual dryness index (E_p/P) for four basins of different climatic conditions. Each data point represents 1 year. It is evident that Fu's expression with different ϖ values is able to capture the interannual variability of the regional water and energy balance for these four basins, as well as for the remaining ones (not shown). It is also clear that at the annual scale, the Budyko curve is basin dependent and ϖ varies significantly across basins. The basin-specific ϖ values are notably different from the default value of 2.6 and the fitted value of 2.0 using long-term averaged data. As a result, accurate estimates of ϖ for different basins are the

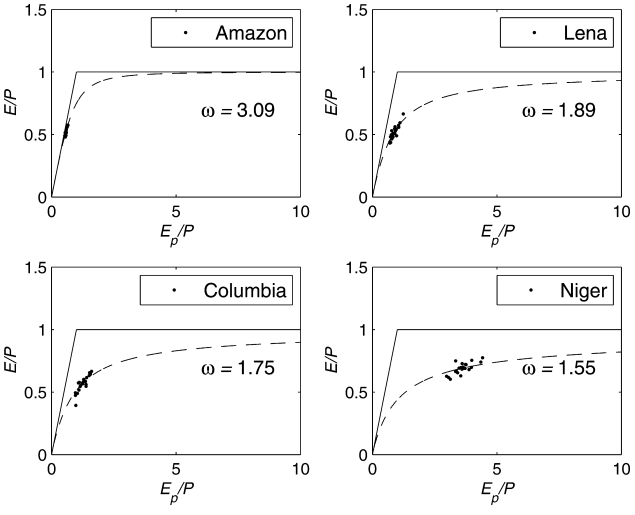

Figure 3. Annual evaporation ratio (E/P) as a function of the annual dryness index (E_p/P) for four basins under different climatic conditions. The black dots are data from *Pan et al*. [2012]. The dotted lines are Fu's equation with the fitted basin-specific ϖ values using the least-square method.

prerequisite for applying the Budyko framework at the annual scale.

3.2. A Simple Parameterization for the Parameter ϖ

[14] In the following analyses, basin-specific ϖ values are first obtained for the 26 basins using the least-square method, as mentioned in section 2.2 (see also Figure 3). Then annual NDVI values for these 26 basins are extracted from the global NDVI data set and averaged over the period from 1984 to 2006, based on which the long-term averaged annual vegetation coverage is calculated using equation (4). As can be seen from Figure 4, the basin-specific ϖ values are well correlated ($R^2 = 0.63$) with the long-term averaged annual vegetation coverage (M). The fitted linear relationship between basin-specific ϖ and the vegetation coverage is:

$$\varpi = 2.36 \times M + 1.16. \tag{6}$$

[15] The positive correlation between ϖ and M implies that basins with larger vegetation coverage generally have higher evaporation ratios (E/P) at a given dryness index, which is in broad consistence with many previous studies [*Donohue et al*., 2007; *Shao et al*., 2012; *Zhang et al*., 2001, 2004]. The new finding here is that in the 26 global river basins examined in this study, it appears that the variability of ϖ is largely captured by the vegetation coverage. As mentioned earlier, there are several reasons that vegetation coverage can serve as a good indicator of the combined ecohydrological impacts on basin-scale water and energy balances. It reflects the influences of climate seasonality, soil properties, and topographic features [*Donohue et al*., 2007; *Williams et al*., 2012; *Zhang et al*., 2001]. The fact that vegetation coverage integrates the effects of these ecohydrological processes on water and energy balances warrants a simple parameterization for ϖ using only vegetation information in the large-scale basins.

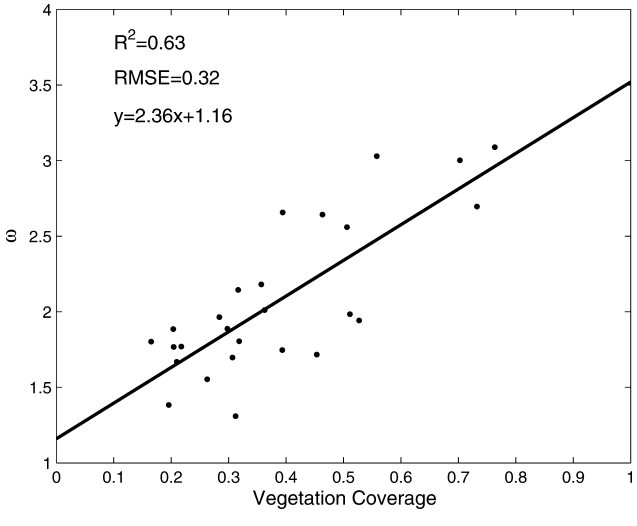

Figure 4. The linear regression between the fitted basin-specific ϖ values and the long-term averaged annual vegetation coverage.

3.3. Validation of the Parameterization for ϖ

3.3.1. Using the Data Set From *Pan et al.* [2012]

[16] The parameterization for the basin-specific ϖ using long-term averaged annual vegetation coverage is given by equation (6). To validate the parameterization, first, the data set from *Pan et al*. [2012] is separated into two groups, one used for calibration and the other used for validation. Due to the limited number of basins in this data set, the group used for validation only consists of 1 basin and the group used for calibration consists of the remaining 25 basins. Nonetheless, this calibration-validation process is rotated so that each time a different basin is used for validation and the remaining 25 are used for calibration. After fitting a linear function between basin-specific ϖ values and the vegetation coverage of the 25 basins, the parameter ϖ for the validation basin is modeled using the fitted function and annual actual evapotranspiration is subsequently computed using Fu's equation with the modeled ϖ.

[17] The modeled annual actual evapotranspiration for the validation basin is compared to data from *Pan et al*. [2012], as shown in Figure 5(c). The modeled annual actual evapotranspiration has a RMSE of 47 mm and a fitted $R^2 = 0.97$ showing the robustness and applicability of the relationship between the basin-specific ϖ parameter and the long-term averaged vegetation coverage. For comparisons, the parameter ϖ values 2.0 (the fitted value using long-term averaged data) and 2.6 (the default value) are also used to calculate the annual actual evapotranspiration using Fu's equation, as shown in Figures 5(a) and 5(b), respectively. It is clear that the proposed parameterization for ϖ improves the actual evapotranspiration modeling as compared to these two estimates by reducing the RMSE from 85 mm and 76 mm to 47 mm, respectively. The RMSE is also calculated for each basin individually and presented in Figure 6. The new parameterization for ϖ reduces the RMSE as compared to the other two methods for most of the basins, with the maximum reduction being from 219 mm ($\varpi = 2.0$) to 70 mm in the Amazon basin. In addition, we also compared the modeled actual evapotranspiration using the fitted basin-specific parameter ϖ, which is the best estimate that can be obtained using Fu's equation, to the actual evapotranspiration reported in *Pan et al*. [2012]. As shown in Figure 5(d), the modeled annual actual evapotranspiration using the basin-specific parameter ϖ yields a RMSE of 21 mm and $R^2 = 0.99$. Consequently, the simple parameterization does not add significant errors into the modeled actual evapotranspiration (comparing Figure 5(c) to Figure 5(d)) and its performance is considered excellent given its simplicity.

[18] Note that the rotated calibrations using 25 basins instead of all 26 basins only produce slight variations in the slopes and intercepts from regressions. For example, the slope varies from 2.22 to 2.48 while the intercept from 1.12 to 1.21. The average of these slope and intercept values are 2.36 and 1.16, respectively, which are identical to the values in equation (6). We also tested another calibration-validation procedure in which more basins (e.g., eight basins) are randomly selected for validation and the remaining basins are used for calibration. The regression is not altered considerably using this alternative procedure, which suggests that the current slope and intercept value in our

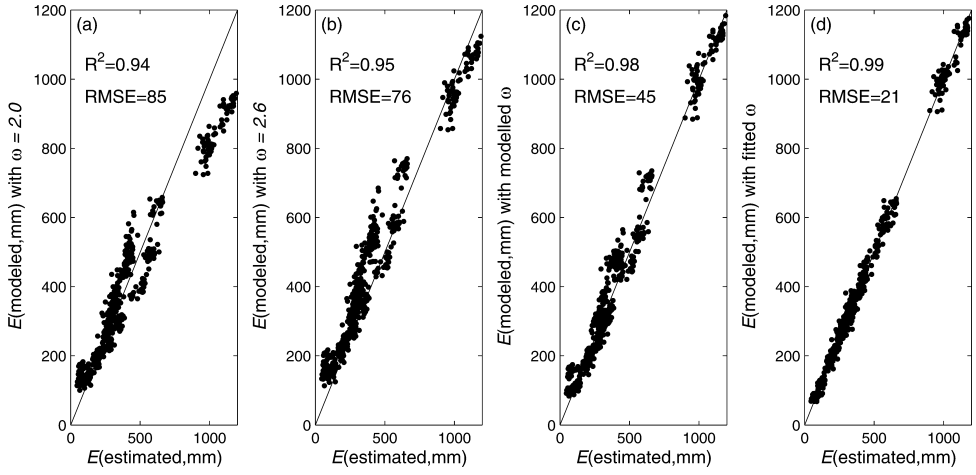

Figure 5. Comparison between the actual evapotranspiration data from *Pan et al*. [2012] and the modeled annual actual evapotranspiration using Fu's equation with (a) $\varpi = 2.0$; (b) $\varpi = 2.6$; (c) the modeled ϖ based on vegetation coverage; (d) the basin-specific ϖ.

parameterization (equation (6)) are robust and adding more basins to the sample pool will not significantly change the results.

3.3.2. Using the Small-Catchment Data Sets

[19] To test how the parameterization in equation (6) applies to small basins, we collected two data sets that include 99 catchments in China and 232 catchments in the United States (the MOPEX data set). The majority of these catchments have sizes ranging from 300 to 50,000 km^2. Figure 7 shows the fitted basin-specific ϖ values normalized by the modeled ϖ_M values $(\varpi_M = 2.36\times\ M + 1.16)$ as a function of basin area. It is clear that in the large basins (larger than 300,000 km^2 in this study), the ratios of ϖ/ϖ_M are close to unity. In the small catchments (smaller than 50,000 km^2 in this study), variations in the basin-specific ϖ values are not entirely controlled by vegetation coverage, and the ϖ/ϖ_M values can be different from unity.

[20] This suggests a diminished impact of vegetation on the basin-specific ϖ parameter in small catchments and is in agreement with some previous studies that also used data collected in small catchments, as can be seen from Figure 4 in *Donohue et al*. [2010], Figure 2 in *Shao et al*. [2012], and Figure 2 in *Yang et al*. [2009]. It also implies that the key ecohydrological processes influencing the water and energy balances are more localized and diverse for small catchments. For example, in order to capture the variations in ϖ in the China data set, two additional variables (i.e., the relative infiltration capacity, $K_s/\overline{i_r}$ and the average topographic slope, $\tan\beta$) need to be taken into consideration. Even so, the parameterization for ϖ is different for the two basins [*Yang et al*., 2009]:

$$\varpi = 5.755\left(\frac{K_s}{\overline{i_r}}\right)^{-0.368} M^{0.292}\exp(-5.428\tan\beta) + 0.72, \quad (7)$$

$$\varpi = 2.721\left(\frac{K_s}{\overline{i_r}}\right)^{-0.393} M^{-0.301}\exp(4.351\tan\beta) + 0.72, \quad (8)$$

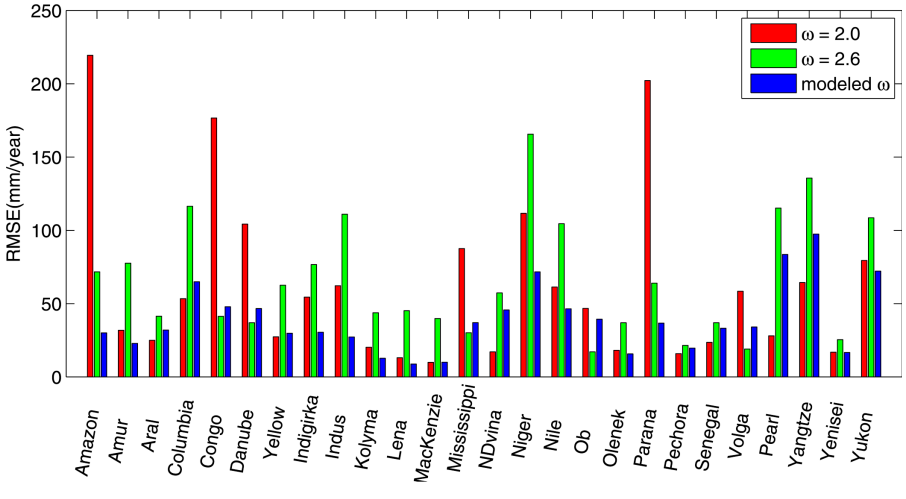

Figure 6. The RMSE between the actual evapotranspiration data from *Pan et al*. [2012] and the modeled annual actual evapotranspiration for each individual basin using Fu's equation with: $\varpi = 2.0$, $\varpi = 2.6$, and the modeled ϖ based on vegetation coverage.

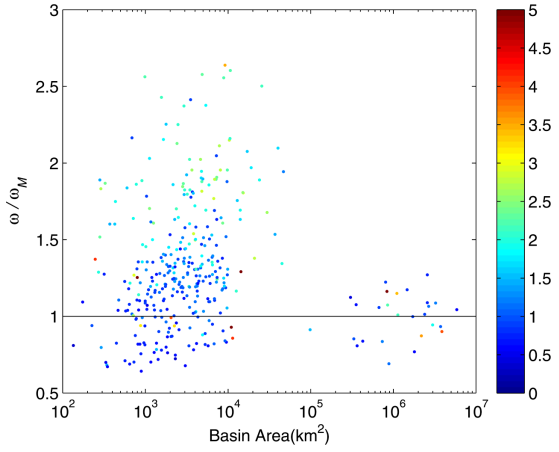

Figure 7. The ratios of the basin-specific ϖ and the modeled ϖ_M ($\varpi_M = 2.36 \times M + 1.16$) are displayed as a function of basin areas. The color bar indicates the long-term averaged annual dryness index E_p/P. It is clear that in large basins, the ϖ/ϖ_M values are close to unity but in small catchments, the ϖ/ϖ_M values can be significantly different from unity.

where equations (7) and (8) are proposed for the Inland River Basin and the Hai River Basin, respectively. A recent study that combines Choudhury's equation with Porporato et al.'s [2004] stochastic soil moisture model shows that the parameter ϖ depends on the mean storm depth within a day ($\overline{i_r}$, mm), the plant-available soil water holding capacity (κ), and the effective rooting depth (Z_e, mm) [*Donohue et al.*, 2012]:

$$\varpi = 0.21 \frac{\kappa Z_e}{\overline{i_r}} + 1.32. \quad (9)$$

[21] Moreover, *Shao et al.* [2012] concluded that the topographic feature (i.e., relief ratio) plays a significant role in affecting the long-term averaged annual evapotranspiration. *Peel et al.* [2010] demonstrated the importance of considering the climatic conditions of the catchments when examining the vegetation impact on actual evapotranspiration. It is plausible that smaller catchments exhibit more heterogeneity in these ecohydrological variables as well as topographic characteristics whose impacts on the parameter ϖ vary across different climatic zones and landscapes. Another reason that small catchments do not exhibit a clear relationship between the basin-specific parameters and the vegetation coverage may be that the non-steady-state condition in these catchments is influential, particularly at annual scales. The water storage changes in these small catchments may need to be explicitly included in the Budyko framework [*Zhang et al.*, 2008].

[22] However, in order not to complicate the parameterization for ϖ, here we only examine the departures of the basin-specific ϖ from the modeled ϖ_M in these small catchments using readily available information such as the dryness index (E_p/P). Figure 7 shows the long-term averaged annual dryness index of each basin or catchment. Close inspection reveals that in the small catchments, the departure of ϖ/ϖ_M from unity is not controlled by the long-term averaged dryness index, suggesting that other factors need to be taken into consideration to explain the departure of ϖ/ϖ_M from unity.

[23] In summary, the vegetation control on water and energy balances is dominant at large spatial scales and a simple parameterization for the basin-specific ϖ parameter based on vegetation information can significantly improve the actual evapotranspiration modeling as compared to the original Budyko curve method in large-scale basins. In small catchments, the interaction between vegetation and the hydrological cycle becomes more complex. Although vegetation may still play a role in modulating water and energy balances in these small catchments, other key parameters have to be taken into consideration in order to fully capture the variability in the basin-specific ϖ parameter. This clearly demonstrates a scale dependence of the role of vegetation in modulating basin-scale water and energy balances.

4. Conclusion

[24] Fu's equation for the Budyko curve is widely used to capture the annual water and energy balances for river basins. However, the parameter ϖ in Fu's equation that controls how much of the available water will be evaporated given the available energy is difficult to estimate. Previous studies have found that land surface characteristics, including vegetation, soil types, and topographic features, have significant impacts on variations in the parameter ϖ. In this study, we only focus on the vegetation impact on the parameter ϖ and examine the conditions under which vegetation plays a major role in controlling the variability of the parameter ϖ. The basin-specific ϖ parameters are obtained using data from the 26 global river basins that are larger than 300,000 km^2 and they are observed to have a good linear relationship with long-term averaged annual vegetation coverage. As such, a simple parameterization for the basin-specific ϖ is proposed based on the long-term averaged annual vegetation coverage. Results indicate that the performance of the parameterization in modeling annual evapotranspiration is good. As shown in Figure 6, the reduction in the RMSE varies across the 26 basins, but overall the new parameterization for ϖ reduces the RMSE by approximately 40% as compared to the original Budyko model ($\varpi = 2.6$).

[25] The controlling impact of vegetation on the basin-specific ϖ parameter is diminished in small catchments ($<$50,000 km^2), which suggests that other key ecohydrological variables such as soil properties, topographic features, and climatic seasonality, may be also of importance. As a result, it is difficult to capture the variability in water and energy balances at small spatial scales by only considering vegetation information, without taking into account the impact of other key ecohydrological processes. Future research involves identifying other critical ecohydrological variables that also affect water and energy balances in small-scale catchments and incorporating them into the Budyko framework. It is also imperative to quantify the water storage changes in the small-scale catchments and evaluate their impacts within the Budyko framework.

[26] **Acknowledgments.** The authors would like to thank Kaiyu Guan and Long Yang for their help in processing the NDVI data set. The research was partially supported by NASA grant NNX08AN40A (Developing Consistent Earth System Data Records for the Global Terrestrial Water Cycle). Cong was supported by the National Natural Science Foundation of China (50909051, 50979039). The authors also thank the three reviewers whose comments helped to improve the paper considerably.

References

Budyko, M. I. (1963), *Evaporation Under Natural Conditions*, v, 130 pp., Isr. Program for Sci. Transl., Off. of Techn. Serv., U.S. Dep. of Commerce, Jerusalem.

Budyko, M. I. (1974), *Climate and Life*, xvii, 508 pp., Acad. Press, New York.

Buermann, W., Y. J. Wang, J. R. Dong, L. M. Zhou, X. B. Zeng, R. E. Dickinson, C. S. Potter, and R. B. Myneni (2002), Analysis of a multiyear global vegetation leaf area index data set, *J. Geophys. Res. Atmos.*, *107*(D22), 4646.

Choudhury, B. J. (1999), Evaluation of an empirical equation for annual evaporation using field observations and results from a biophysical model, *J. Hydrol.*, *216*(1–2), 99–110.

Donohue, R. J., M. L. Roderick, and T. R. McVicar (2007), On the importance of including vegetation dynamics in Budyko's hydrological model, *Hydrol. Earth Syst. Sci.*, *11*(2), 983–995.

Donohue, R. J., M. L. Roderick, and T. R. McVicar (2010), Can dynamic vegetation information improve the accuracy of Budyko's hydrological model? *J. Hydrol.*, *390*(1–2), 23–34.

Donohue, R. J., M. L. Roderick, and T. R. McVicar (2011), Assessing the differences in sensitivities of runoff to changes in climatic conditions across a large basin, *J. Hydrol.*, *406*(3–4), 234–244.

Donohue, R. J., M. L. Roderick, and T. R. McVicar (2012), Roots, storms and soil pores: Incorporating key ecohydrological processes into Budyko's hydrological model, *J. Hydrol.*, *436*, 35–50.

Duan, Q., et al. (2006), Model Parameter Estimation Experiment (MOPEX): An overview of science strategy and major results from the second and third workshops, *J. Hydrol.*, *320*(1–2), 3–17.

Eagleson, P. S. (2002), *Ecohydrology: Darwinian Expression of Vegetation Form and Function*, vol. 39, 443 pp., Cambridge Univ. Press, Cambridge, U. K.

Fu, B. P. (1981), On the calculation of the evaporation from land surface [in Chinese], *Sci. Atmos. Sin.*, *5*(1), 23–31.

Gutman, G., and A. Ignatov (1998), The derivation of the green vegetation fraction from NOAA/AVHRR data for use in numerical weather prediction models, *Int. J. Remote Sens.*, *19*(8), 1533–1543.

Ma, Z. M., S. Z. Kang, L. Zhang, L. Tong, and X. L. Su (2008), Analysis of impacts of climate variability and human activity on streamflow for a river basin in arid region of northwest China, *J. Hydrol.*, *352*(3–4), 239–249.

Milly, P. C. D. (1993), An analytic solution of the stochastic storage problem applicable to soil-water, *Water Resour. Res.*, *29*(11), 3755–3758.

Milly, P. C. D. (1994), Climate, soil-water storage, and the average annual water-balance, *Water Resour. Res.*, *30*(7), 2143–2156.

Owe, M., R. de Jeu, and J. Walker (2001), A methodology for surface soil moisture and vegetation optical depth retrieval using the microwave polarization difference index, *IEEE Trans. Geosci. Remote Sens.*, *39*(8), 1643–1654.

Pan, M., and E. F. Wood (2006), Data assimilation for estimating the terrestrial water budget using a constrained ensemble Kalman filter, *J. Hydrometeorol.*, *7*(3), 534–547.

Pan, M., A. K. Sahoo, T. J. Troy, R. K. Vinukollu, J. Sheffield, and E. F. Wood (2012), Multisource estimation of long-term terrestrial water budget for major global river basins, *J. Clim.*, *25*(9), 3191–3206.

Peel, M. C., T. A. McMahon, and B. L. Finlayson (2010), Vegetation impact on mean annual evapotranspiration at a global catchment scale, *Water Resour. Res.*, *46*, W09508, doi:10.1029/2009WR008233.

Porporato, A., E. Daly, and I. Rodriguez-Iturbe (2004), Soil water balance and ecosystem response to climate change, *Am. Nat.*, *164*(5), 625–632.

Roderick, M. L., and G. D. Farquhar (2011), A simple framework for relating variations in runoff to variations in climatic conditions and catchment properties, *Water Resour. Res.*, *47*, W00G07, doi:10.1029/2010WR009826.

Rodríguez-Iturbe, I., and A. Porporato (2004), *Ecohydrology of Water-Controlled Ecosystems: Soil Moisture and Plant Dynamics*, vol. 18, 442 pp., Cambridge Univ. Press, Cambridge, U. K.

Shao, Q. X., A. Traylen, and L. Zhang (2012), Nonparametric method for estimating the effects of climatic and catchment characteristics on mean annual evapotranspiration, *Water Resour. Res.*, *48*, W03517, doi:10.1029/2010WR009610.

Sheffield, J., and E. F. Wood (2007), Characteristics of global and regional drought, 1950–2000: Analysis of soil moisture data from off-line simulation of the terrestrial hydrologic cycle, *J. Geophys. Res. Atmos.*, *112*, D17115, doi:10.1029/2006JD008288.

Sheffield, J., G. Goteti, and E. F. Wood (2006), Development of a 50-year high-resolution global dataset of meteorological forcings for land surface modeling, *J. Clim.*, *19*(13), 3088–3111.

Shuttleworth, W. J. (1993), Evaporation, in *Handbook of Hydrology*, edited by D. R. Maidment, pp. 4.1–4.53, McGraw-Hill, New York.

Sun, F. B. (2007), *Study on watershed evapotranspiration based on the Budyko hypothesis [in Chinse], Ph.D. thesis*, Tsinghua Univ., Beijing.

Wang, D. B., and N. Alimohammadi (2012), Responses of annual runoff, evaporation, and storage change to climate variability at the watershed scale, *Water Resour. Res.*, *48*, W05546, doi:10.1029/2011WR011444.

Wang, D. B., and M. Hejazi (2011), Quantifying the relative contribution of the climate and direct human impacts on mean annual streamflow in the contiguous United States, *Water Resour. Res.*, *47*, W00J12, doi:10.1029/2010WR010283.

Williams, C. A., et al. (2012), Climate and vegetation controls on the surface water balance: Synthesis of evapotranspiration measured across a global network of flux towers, *Water Resour. Res.*, *48*, W06523, doi:10.1029/2011WR011586.

Yang, D. W., F. B. Sun, Z. Y. Liu, Z. T. Cong, G. H. Ni, and Z. D. Lei (2007), Analyzing spatial and temporal variability of annual water-energy balance in nonhumid regions of China using the Budyko hypothesis, *Water Resour. Res.*, *43*, W04426, doi:10.1029/2006WR005224.

Yang, D. W., W. W. Shao, P. J. F. Yeh, H. B. Yang, S. Kanae, and T. Oki (2009), Impact of vegetation coverage on regional water balance in the nonhumid regions of China, *Water Resour. Res.*, *45*, W00A14, doi:10.1029/2008WR006948.

Yang, H. B., and D. W. Yang (2011), Derivation of climate elasticity of runoff to assess the effects of climate change on annual runoff, *Water Resour. Res.*, *47*, W07526, doi:10.1029/2010WR009287.

Yang, H. B., D. W. Yang, Z. D. Lei, and H. M. Lei (2008a), Derivation and validation of watershed coupled water-energy balance equation at arbitrary time scale [in Chinese], *J. Hydraulic Eng.*, *39*(5), 610–617.

Yang, H. B., D. W. Yang, Z. D. Lei, and F. B. Sun (2008b), New analytical derivation of the mean annual water-energy balance equation, *Water Resour. Res.*, *44*(3), W03410, doi:10.1029/2007WR006135.

Yokoo, Y., M. Sivapalan, and T. Oki (2008), Investigating the roles of climate seasonality and landscape characteristics on mean annual and monthly water balances, *J. Hydrol.*, *357*(3–4), 255–269.

Zhang, L., W. R. Dawes, and G. R. Walker (2001), Response of mean annual evapotranspiration to vegetation changes at catchment scale, *Water Resour. Res.*, *37*(3), 701–708.

Zhang, L., K. Hickel, W. R. Dawes, F. H. S. Chiew, A. W. Western, and P. R. Briggs (2004), A rational function approach for estimating mean annual evapotranspiration, *Water Resour. Res.*, *40*, 02502, doi:10.1029/2003WR002710.

Zhang, L., N. Potter, K. Hickel, Y. Q. Zhang, and Q. X. Shao (2008), Water balance modeling over variable time scales based on the Budyko framework–Model development and testing, *J. Hydrol.*, *360*(1–4), 117–131.